Design of suspension control system for bearingless induction motor using fuzzy-I controller

Qasim Kadhim Jasim, Mohammed Moanes E. Ali
Department of Electrical Engineering, University of Technology, Baghdad, Iraq

Article Info

ABSTRACT

In the bearingless induction motor (BIM), the rotor of BIM is supported by the magnetic force, the radial position control technique is studied in this paper, an approximation and simplification are used to create a linearized model of suspension system. The objective of this paper is to design a control system that overcomes the limitations of the traditional controller and to improve the control performance and achieve high stability, even if it is exposed to external disturbance and internal disturbance (changes in load or speed). In order to solve this problem, the proposed controller is based on the fuzzy-I controller that combines the positive features of both fuzzy logic and the integration. In comparison with the conventional PID, the results show that the fuzzy-I controller reduces the peak-to-peak rotor deviation by 23% under effect of external disturbance force and 31% under effect of speed variation and 9% under effect of load variation.

Corresponding Author:

Qasim Kadhim Jasim
Department of Electrical Engineering, University of Technology
Baghdad, Iraq
Email: eee.20.70@grad.uotechnology.edu.iq

1. INTRODUCTION

A mechanical bearings motor is unable to meeting the requirements for high speed and long-term operation. As a result, the magnetic bearing motor was created. However, the magnetic bearing motor has many disadvantages such as complex structure, high energy consumption for the magnetic suspension, low efficiency, difficulty of over-speed and so on [1], [2]. The bearingless motor is the best solution for this problem where the number of the inverters, dimensions of the motor, and the associated costs are reduced [3], [4].

There are many types of the bearingless motor, the bearingless induction motor is one of the most important of these types. The BIM is a hybrid of conventional motor and magnetic bearing, The BIM consists of two set of windings are imbedded in stator slots, the electromagnetic torque windings to generates rotation torque and the suspension control windings to control the suspension force [5]–[8]. A magnetic levitation force is generated by the interaction of the air-gap magnetic flux generated by two sets of the stator windings, used to control the axial suspension force of the rotor [1]. Compared with magnetic bearing, the bearingless motor has many advantages, like higher critical speed, shorter shaft, smaller in size, and lower cost [9]. In a bearingless induction motors, the volt-Ampere required for axial levitation force control is very small compared with the volt-Ampere of torque windings [4]. This result indicates possible cost reduction in the bearingless induction motor and demonstrates it is less expensive. The induction motor has many advantages over other types of motors such as its robustness, low cost and its simplicity [10].

The important problems and requirements for controlling BIM is to generate an electromagnetic force in order to prevent the collision between the stator and the rotor that makes the rotor rotates in the center of

stator bore. A sliding mode controller with variable structures of BIM was proposed by [11] to implement the dynamic decoupling control with excellent performance and enhance the stability of the system. Direct torque and the suspension forces control for BIM using active disturbance rejection controller was proposed [12], the simulation and testing findings demonstrate that the ADRC technique has excellent robustness, can effectively reduce the influence of the load disturbance and also reduce overshoot. Direct levitation force control method using model prediction has been proposed by [13], the modeling and experiment results demonstrate that the suggested control technique can successfully increase the suspension stability of the rotor also enhancing the system's ability to resist disturbances. The non-singular fast terminals with sliding mode control was proposed in [14], The experiment and simulation result demonstrate that the proposed controller tracks the values of the radial displacement and speed quickly, also, the rotor is reaching to the steady state position immediately and achieving stability.

       The goal of this paper is to design control system to overcome the traditional controller limitations and to improve control performance and achieve high system stability even when the motor shaft is subjected to external disturbances. The proposed control system in this work is based on the fuzzy-I controller: this controller combines the features of both fuzzy and integration. fuzzy logic is a nonlinear control system, it doesn't require exact mathematical models and the integration helps to reduce the steady state error.

2. MATHMATICAL MODELS OF BEARINGLESS INDUCTION MOTOR

       The BIM contains two groups of stator winding are embedded in the same slots. In this work, the following structure is considered: four poles winding p_1 to generate the electromagnetic torque and two poles winding p_2 to generate the rotor suspension forces as shown in Figure 1. The two groups must achieve two important conditions in order to generate stable suspension force: $\omega_1=\omega_2$ and $P_1=P_2\pm1$, where ω_1 and ω_2 represent the angular frequencies of torque and suspension windings respectively.

       Figure 2 Shows that the flux linkage in air-gab Ψ_1 and Ψ_2 are generated by the current of torque windings 1a and suspension windings 2a respectively, Ψ_1 and Ψ_2 are in same direction on the left side of air-gap, Ψ_1 and Ψ_2 are in opposite direction in right side of air-gap, as a result the magnetic flux density in left side is greater than the magnetic flux density on the right side, then the radial levitation force F is generated in the negative X axis. If the currents in radial suspension windings are reversed, a radial levitation force is generated in the positive X axis. In the same way the radial levitation force in Y direction is controlled by supplying current in the suspension windings 2b which are perpendicular to the suspension windings 2a [15].
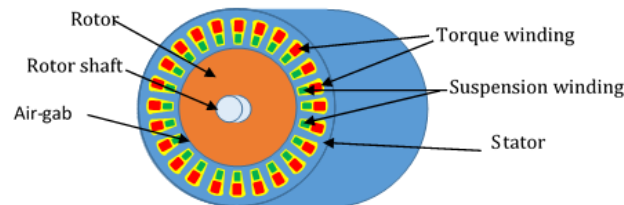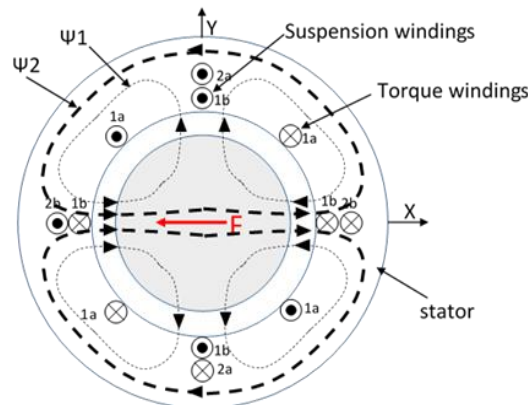

Figure 1. Structure of BIM

Figure 2. Principle of radial the suspension forces generation

2.1. Electromagnetic torque and speed of BIM

The magnetic flux of the axial suspension windings and torque windings induce a current in the rotor, however, the current induced by the suspension windings and torque that caused by it can be ignored because it is very small with respect to the current induced by torque windings, so the magnetic flux of the air-gap can be written as [14]–[16]:

$$\psi_{1d} = L_{1m}(I_{1ds} + I_{1dr}) \tag{1}$$

$$\psi_{1q} = L_{1m}(I_{1qs} + I_{1qr}) \tag{2}$$

where: Ψ_{1d} and Ψ_{1q} are the flux linkage in air-gab in d-q coordinates system respectively, L_{1m} is mutual inductance for torque windings, i_{1dr}, i_{1qr}, i_{1ds} and i_{1qs} are the rotor and stator current components for torque winding by the d-q coordinates system respectively. We can write the relationship of electromagnetic torque as follows:

$$Te = P_1(I_{1qs}\psi_{1d} - I_{1ds}\psi_{1q}) \tag{3}$$

where: P1 is the pair of poles for torque windings.

In this work the field-oriented control system (FOC) is used of the BIM speed control, this system also enables the flux and torque of BIM to be controlled separately as in separately excited DC motor, in other words, the electric torque is controlled by the i_{1qs} current and the flux by the i_{1ds} current. By using rotor field-oriented control scheme, the vector of rotor field for torque winding is aligned in the direct axis, that means the linkage flux components of the rotor for torque winding will be: $\Psi_{qr} = 0$ and $\Psi_{dr} = \Psi r$ [2], [17].

$$i_{1ds}{}^* = \frac{\Psi_{1r}{}^*}{L_m} \tag{4}$$

$$i_{1qs}{}^* = \frac{L_{1r}Te^*}{P_1 L_{1m}\ \Psi_{1r}{}^*} \tag{5}$$

Depending of the machine parameters the slip speed can be write as (6).

$$\omega_{sl} = \frac{L_{1m}R_{1r}i_{1sq}{}^*}{L_{1r}\ \Psi_{1r}{}^*} \tag{6}$$

From the measured speed of the rotor (ω_r) and slip speed (ω_{sl}) can be obtained the flux transformation angle (θ) as follows:

$$\theta = \int (\omega_{sl} + \omega_r)dt \tag{7}$$

from basic equations of rotor.

$$\psi_r = \frac{I_{1ds}}{Lm}(1 + \tau p) \tag{8}$$

The electromagnetic torque equation can be determined as:

$$Te = P_1 \frac{L_{1m}}{L_{1r}}(I_{1qs}\psi_r) \tag{9}$$

where: L_{1r} is the inductance of the rotor for torque winding, R_{1r} is the resistance of the rotor for torque winding, p is the partial derivative, τ is rotor time constant, TL is the load torque, J and P_1 are moment of inertia and pole pairs for torque winding respectively.

2.2. Suspension forces of bearingless induction motor

Two-poles suspension force winding and four-pole torque winding are embedded in stator slots of the BIM. The electromagnetic coupling of the bearingless induction motors is very complex, because the coupling between the two-pole winding and four-pole windings, and the couplings between the stator windings

themselves. So, to deal with this form easily, the three phase (abc) is transformed to a two-phase system (αβ) and then transformed to a two-phase rotation system (dq). Let Ψ_{2a}, Ψ_{2b}, Ψ_{1a} and Ψ_{1b} are the flux linkage of windings: 2a, 2b, 1a and 1b respectively and i_{2ds}, i_{2qs}, i_{1ds} and i_{1qs} are the stator current components in d-q coordinates of windings 2a, 2b, 1a and 1b respectively. The flux linkage equations of the BIM can be written as follows [18]–[21]:

$$[\Psi] = [L] * [i] \tag{10}$$

$$\begin{bmatrix} \Psi_{1a} \\ \Psi_{1b} \\ \Psi_{2a} \\ \Psi_{2b} \end{bmatrix} = \begin{bmatrix} L_{1a} & M_{1a1b} & M_{1a2a} & M_{1a2b} \\ M_{1b1a} & L_{1b} & M_{1b2a} & M_{1b2b} \\ M_{2a1a} & M_{2a1b} & L_{2a} & M_{2a2b} \\ M_{2b1a} & M_{2b1b} & M_{2b2a} & L_{2b} \end{bmatrix} * \begin{bmatrix} i_{1ds} \\ i_{1qs} \\ i_{2ds} \\ i_{2qs} \end{bmatrix} \tag{11}$$

where: M and L is the mutual and self-inductance and subscript of 1 and 2 refer to torque winding and suspension windings respectively. The value of mutual inductance between four- pole windings with themselves is zero, the value of mutual inductance between the two-pole windings with themselves is zero, the value of self-inductance for torque windings (L_{1s}) and the suspension windings (L_{2s}) are constant, only the value of mutual-inductance between the torque winding and the suspension windings is variable and dependent of the rotor displacement variation in X and Y direction, So the equation of inductance matrix for the (BIM) can be written as [20]:

$$[L] = \begin{bmatrix} L_{1s} & 0 & -\acute{M}X & \acute{M}Y \\ 0 & L_{1s} & \acute{M}Y & \acute{M}X \\ -\acute{M}X & \acute{M}Y & L_{2s} & 0 \\ \acute{M}Y & \acute{M}X & 0 & L_{2s} \end{bmatrix} \tag{12}$$

where M´ is mutual inductance coefficient for fore-pole windings and two-pole windings, X and Y are radial displacement of rotor in X and Y axis respectively. According to the principle of energy conversion in the BIM, we can describe the magnetic energy that is stored in the stator windings as follows [21]:

$$[w] = \frac{1}{2} * [i]^T [L][i] \tag{13}$$

By neglecting magnetic flux saturation, the axial forces Fx = dw/dx in X direction and Fy = dw/dy in Y direction as follows:

$$\begin{bmatrix} Fx \\ Fy \end{bmatrix} = \begin{bmatrix} \frac{dw}{dx} \\ \frac{dw}{dy} \end{bmatrix} = \acute{M} \begin{bmatrix} -i_{1ds} & i_{1qs} \\ i_{1qs} & i_{1ds} \end{bmatrix} \begin{bmatrix} i_{2ds} \\ i_{2qs} \end{bmatrix} \tag{14}$$

$$\text{Let, } i_{1ds} = I_m * \cos(\omega t) \tag{15}$$

$$i_{1qs} = I_m * \sin(\omega t) \tag{16}$$

then

$$\begin{bmatrix} Fx \\ Fy \end{bmatrix} = \acute{M} * I_m \begin{bmatrix} -\cos(\omega t) & \sin(\omega t) \\ \sin(\omega t) & \cos(\omega t) \end{bmatrix} \begin{bmatrix} i_{2ds}{}^* \\ i_{2qs}{}^* \end{bmatrix} \tag{17}$$

where: I_m is the magnetizing current of the torque windings.

2.3. The radial motion equations of the suspended rotor

In this section, we will study the axial (radial) motion of the rotor based on the newton's second law, which states that the sum of the forces that act on the rotor are equal to the product of mass multiplied by acceleration, the radial motion equations of rotor shaft in the X and Y directions as shown in Figure 3 can be written as [1], [22]:

$$\text{Fdx} + \text{Fsx} + \text{Fx} = m\ddot{X} \tag{18}$$

$$\text{Fdy} + \text{Fsy} + \text{Fy} = m\ddot{Y} \tag{19}$$

$$Fsx = Ks\ X \text{ and } Fsy = Ks\ Y$$

$$Ks = \frac{l\ r\ \pi\ B^2}{2\mu_0\ g} \tag{20}$$

where: m, l and r are the mass, length and radius of rotor respectively, Fsx, Fsy are unilateral magnetic pull components along x and y direction respectively, Ks represents radial displacement stiffness factor, B is magnetic-flux density, g is the length of air-gap, μ_0 is the vacuum permeability and Fdx, Fdy are the external disturbance of the rotor in X and Y axis direction respectively.
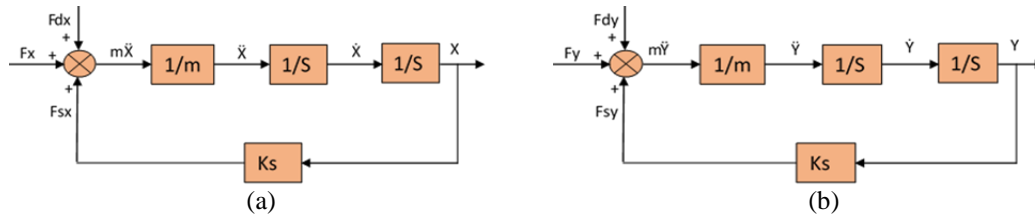

Figure 3. State space of rotor motion in (a) X axis and (b) Y axis

3. THE PROPOSED CONTROLLER (FUZZY-I)

The proposed control system is simulated by using the MATLAB-Simulink platform as shown in Figure 4. This control system is divided into two subsystems for rotation torque control and suspension control. The rotation of the motor is controlled by using the field-oriented control system (FOC), while the axial suspension forces in the X and Y axis are controlled by using the differences between the references and measured values of rotor position, which are adjusted by using the fuzzy-I controller. The adjustable suspension currents $i_{2d}*$ and $i_{2q}*$ are obtained by converting the forces Fx and Fy to currents using the equation of modulation as (21) [20].

$$\begin{bmatrix} i_{2d}^* \\ i_{2q}^* \end{bmatrix} = \begin{bmatrix} -\cos(2\omega_0)t & \sin(2\omega_0)t \\ \sin(2\omega_0)t & \cos(2\omega_0)t \end{bmatrix} \begin{bmatrix} F_x^* \\ F_y^* \end{bmatrix} \tag{21}$$
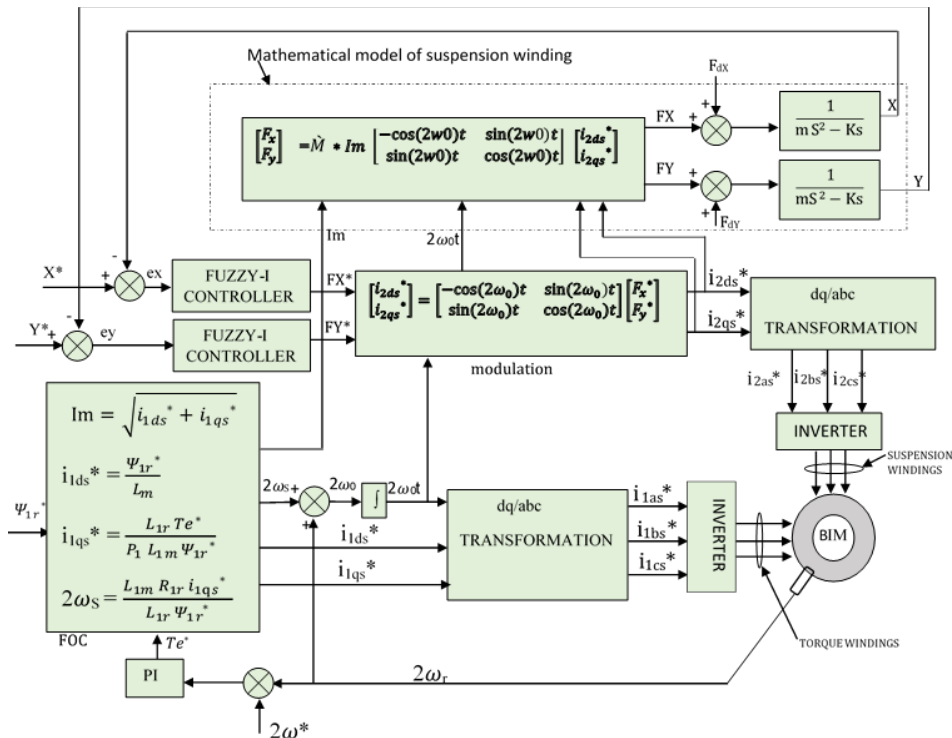

Figure 4. Block diagram of the presented control system

By using dq-abc transformation the three reference currents of suspension force are determined. The suspension windings are supplied by three phase bridge inverter and the current of each phase is controlled separately, this is simply achieved by comparison the reference currents (i_S*) to the actual currents (i_S) by using the hysteresis comparator as shown in Figure 5. In the bearingless induction motor, a new set of windings has been added with the main stator windings. The purpose of these additional windings is to keep the rotor in the center and away from the stator, which are controlled by the separate control system.
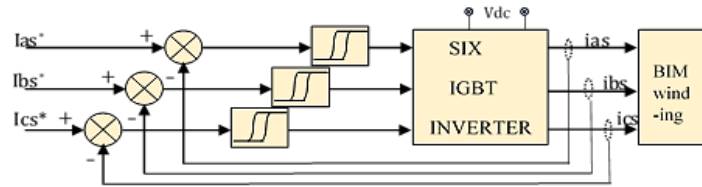

Figure 5. Current controller of induction motor

Many well-known structures are employed in design of the PID-like fuzzy logic controller depending on the structure used, fuzzy-I control system has been proposed in this paper. The structure is fuzzy logic connected in parallel with integration. This controller combines the features of both fuzzy and integration. Figure 6 illustrates the diagram of the fuzzy-I control system; two of these controllers are used, one for controlling the X position of the rotor and the other for Y position.
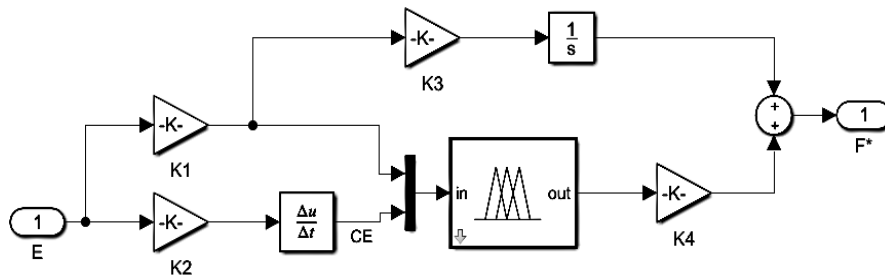

Figure 6. The simulation of fuzzy-I controller

K1 and K2 are selected based on the limits of error and the change in error to be suitable to the range of the fuzzy logic input, K3 and K4 are selected to improve the control system performance by using trial and error. The main structure of the fuzzy logic system includes three stages, the fuzzification, Inference rules, and defuzzification stage. In fuzzification, the data of input are converted to the fuzzy values, which are lingual values understandable by inference mechanism, where fuzzification is the process of applying membership functions to input variables. The inference rule employs fuzzy operations to map the input linguistic value to the output linguistic values. In the defuzzification, the fuzzy values which are resulting from the inference are transformed to crisp values [23], [24].

The fuzzy logic employed in this study consists of two inputs, the error of displacement (E) and change in error (CE), each one of the inputs and outputs has a membership function. The input and lingual variables are NB (negative big), NM (negative medium), NS (negative small), Z (zero), PS (positive small), PM (positive medium), and PB (positive big) where, the universe(rang) of both error and the change in error is [-1 1] as shown in Figure 7. There are six different kinds of membership function which are trapezoidal, triangular, Gaussian, sigmoidal, s-type and z-type. For input: triangle, s-type and z-type are used, while for output, triangle shape is used, this combination gives most accurate results compared with other kinds of the membership functions.

The lingual variables of the output are NB (negative big), NM (negative medium), NS (negative small), Z (zero), PS (positive small), PM (positive medium), and PB (positive big) and their input range(universe) of [-1 1]. The arrangement of the output membership functions is shown in Figure 8. The fuzzy rules are statements set of IF-THEN used to determine the output state from the input state [25], the rules of the fuzzy control system are tabulated in Table 1.
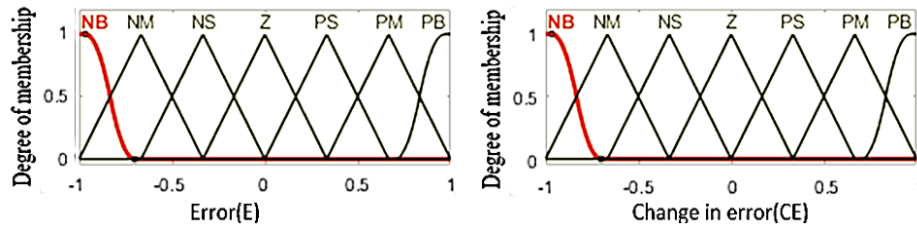
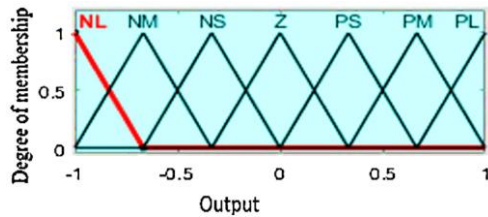Figure 7. Input membership functions (a) E (error) and (b) CE (change in error)

Figure 8. The output membership functions

Table 1. Fuzzy rule

E \ CE	NB	NM	NS	Z	PS	PM	PB
NB	NL	NL	NM	NM	NS	NS	Z
NM	NL	NL	NM	NS	NS	Z	PS
NS	NM	NM	NS	Z	Z	PS	PS
Z	NM	NS	Z	Z	Z	PS	PM
PS	NS	NS	Z	Z	PS	PM	PM
PM	NS	Z	PS	PS	PM	PL	PL
PB	Z	PS	PS	PM	PM	PL	PL

4. RESULTS OF SIMULATION

To effectively verify the proposed controller, a system of bearingless three-phase induction motor is simulated and analyzed at different operating conditions. In this section the results of the proposed control system are compared with conventional PID results. The rotor deviation should not exceed 50 percent from the length of air-gap (0.6 mm) to prevent the collision with the stator. The parameters of BIM are tabulated in Table 2.

Table 2. BIM parameters [26]

Symbols	Value	Description	Symbols	Value	Description
Lm1	0.1586	Mutual inductance for torque-windings (H)	m	2.86	Mass of the rotor (Kg)
L1r	0.0092	Leakage inductance of the rotor (H)	N1	60	No. of turn for torque windings
R1r	11.48	Resistance of rotor (Ω)	N2	140	No. of turn for suspension windings
J	0.00796	Moment of inertia (Kg.m^2)	P1	2	Pole-pairs for torque windings
l	105	Long of the rotor (mm)	P2	1	Pole-pairs for suspension windings
r	97.8	diameter of the rotor (mm)	g	0.6	Air-gab (mm)

The motor is started at reference speed of 3000 rpm and load torque TL=2 Nm and no external disturbance forces on rotor shaft. At time 0.2 s, an external-disturbance force in negative X axis direction of 40 N is applied on the rotor as shown in Figure 9(a). Figure 9(b) shows the rotor deviation from the center point in the X axis direction at time 0.2 s. The value of the maximum rotor deviation is 160 μm by using a conventional PID controller and 88 μm by using proposed fuzzy-I controller and the peak-to-peak rotor deviation is 160 μm by using a conventional PID controller and 123 μm by using the proposed fuzzy-I controller. at time 0.2 s the radial suspension force (Fx) will increase from zero to 40N to overcome the external disturbance force as shown in Figure 9(c). Figure 9(d) shows the peak to peak three phase current of suspension windings, before the disturbance force is applied, the suspension windings current is 90 mA to counter the rotor weight and then at time 0.2 s the suspension current is increased to 145 mA to counter both of the rotor weight and the external-disturbance force.

To verify the suspension control system performance during the variation of reference speed, at time 0.5 s the reference-speed (ω^*) is increased from 3000 to 4000 rpm (314 to 419 rad/s) as shown in Figure 10(a). The speed of the rotor (ωr) reaches a steady state after 27 ms. Figure 10(b) shows the effect of the speed variation of rotor position in X axis direction, the value of the maximum rotor deviation is 100 μm by using a conventional PID controller and 53 μm by using proposed fuzzy-I controller and the peak-to-peak rotor deviation is 138 μm by using a conventional PID controller and 95 μm by using the proposed fuzzy-I controller. Figure 10(c) shows the effect of the speed variation of rotor position in Y axis direction, the maximum value of rotor deviation is 78 μm with traditional PID, this deviation decreases to 40 μm by using the proposed fuzzy-I controller. Figure 10(d) shows the effect of speed variation on the suspension current, the motor current increases during the acceleration period, which leads to a decrease in suspension current from 145 mA to 30 mA (peak to peak value) because the suspension current is inversely proportional to the load current in the event that the suspension force is constant. When the speed reaches to the steady state, the suspension current returns to the normal value (145 mA).
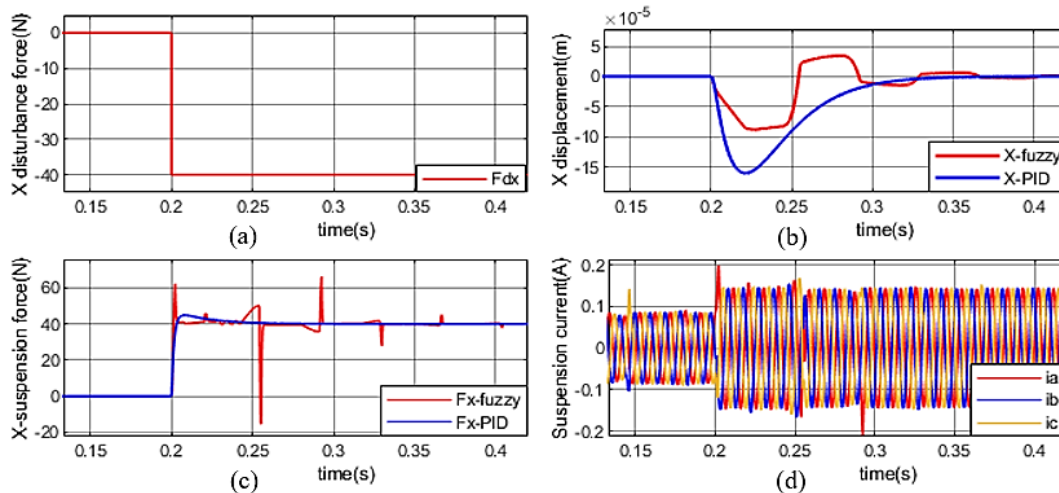
Figure 9. Performance of control system during disturbance force: (a) disturbance force, (b) X- displacement, (c) X-suspension force, and (d) the suspension current
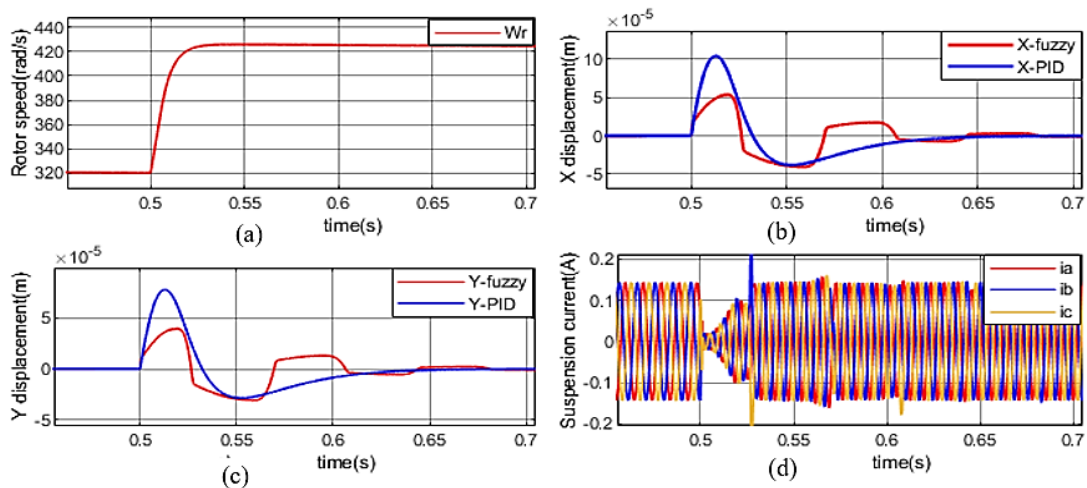

Figure 10. Effect of the speed change: (a) the rotor speed, (b) X displacement, (c) Y displacement, and (d) the suspension current

In case of speed and torque variation the displacement value towards the X axis is greater than the displacement towards the Y axis, because the displacement towards the X axes is affected by the force applied towards the X axis (disturbance force) which is equal to 40N, and the displacement towards the Y axis is affected by the rotor weight (28.5 N).

To verify the suspension control system performance during the variation of load torque, at time 0.9 s the load torque is increased from 2 to 10 Nm as shown in Figure 11(a). Figure 11(b) shows the effect of load variation of rotor position in X axis direction, the maximum rotor deviation is 43 µm by using a conventional PID controller and 30 µm by using the proposed fuzzy-I controller and the peak-to-peak rotor deviation is 43 µm by using a conventional PID controller and 39.1 µm by using proposed fuzzy-I controller. Figure 11(c) shows the effect of load variation on rotor position in Y axis direction, the maximum rotor deviation is 32 µm using PID, this deviation decreases to 22 µm by using the fuzzy-I controller. Figure 11(d) shows effect of the load variation on the suspension current, the load current increases with the increase of load, which leads to a decrease in suspension current from 145 mA to 103 mA (peak to peak value), because the suspension current is inversely proportional to the load current when the suspension force is constant.

Summary of results and a comparison between the conventional PID and the fuzzy-I controller based on the peak-to-peak rotor deviation in X axis direction are shown in the Table 3. The percentage deviation is calculated by (22).

$$\text{Percentage deviation } \% = \frac{\text{peak to peak deviation with PID} - \text{peak to peak deviation with Fuzzy\_I}}{\text{peak to peak deviation with PID}} \qquad (22)$$

The simulation results show that the peak-to-peak rotor deviation by using fuzzy-I controller is decreased compared with conventional PID so the fuzzy-I controller is more suitable to control the radial suspension system of bearingless induction motor.
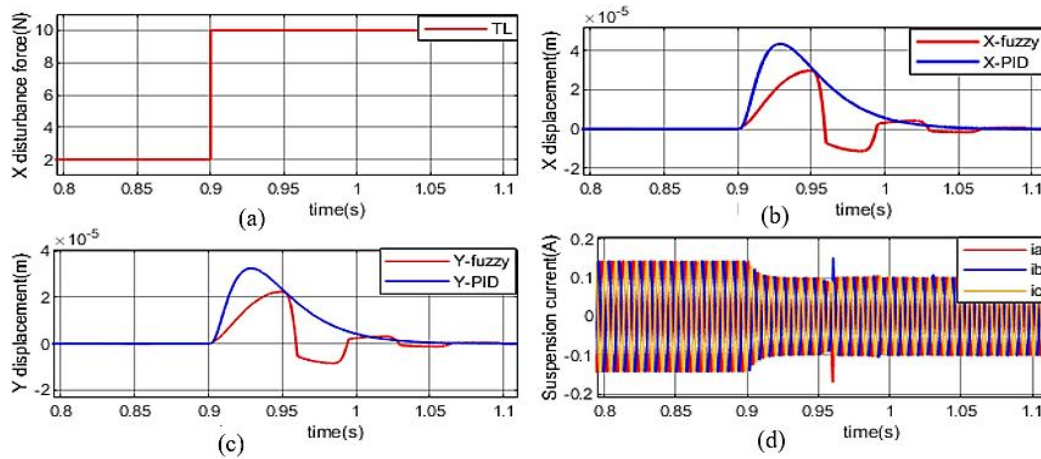

Figure 11. Effect of load torque variation: (a) load torque, (b) X displacement, (c) Y displacement, and (d) the suspension current

Table 3. Rotor deviation in X axis with effect of different conditions

	Disturbance force effect	Speed variation effect	Load torque variation effect
Maximum deviation with PID	160 (µm)	100 (µm)	43 (µm)
Maximum deviation with fuzzy-I	88 (µm)	53 (µm)	30 (µm)
Peak to peak deviation with PID	160 (µm)	138 (µm)	43 (µm)
Peak to peak deviation with fuzzy-I	123 (µm)	95 (µm)	39.1 (µm)
Percentage decrease of deviation	23	31	9

5.   CONCLUSION

The rotor of the BIM is supported by magnetic forces, the modelling of these forces is complex. In general, approximation and simplification are used to create a linearized model in order to assess the performance of the proposed controllers. The proposed suspension controller is based on fuzzy-I controller, the fuzzy logic controller is nonlinear system and doesn't require exact mathematical models and the integration helps to reduce the steady state error. The simulation of the suspension control system shows that the fuzzy-I controller reduces the peak-to-peak rotor deviation by 23% under effect of external disturbance, 31% under effect of speed variation, and 9% under effect of load variation, this percentage decrease of deviation for the rotor position were found through the peak-to-peak deviation values. The propitious results certify the applicability of fuzzy-I to control the radial suspension system of bearingless induction motor.

REFERENCES

[1] Y. Chen, W. Bu, and Y. Qiao, "Research on the speed sliding mode observation method of a bearingless induction motor," *Energies*, vol. 14, no. 4, 2021, doi: 10.3390/en14040864.

[2] C. X. Duan, Y. Han, and Y. H. Zhao, "Design of suspension control system for bearingless motor," in *Advanced Materials Research*, 2012, vol. 538, pp. 3277–3280.

[3] N. Mamat, K. Abdul Karim, Z. Ibrahim, T. Sutikno, S. A. A. Tarusan, and A. Jidin, "Bearingless permanent magnet synchronous motor using independent control," *International Journal of Power Electronics and Drive Systems*, vol. 6, no. 2, pp. 233–241, 2015, doi: 10.11591/ijpeds.v6.i2.pp233-241.

[4] T. Suzuki, A. Chiba, M. A. Rahman, and T. Fukao, "An air-gap-flux-oriented vector controller for stable operation of bearingless induction motors," *IEEE Transactions on Industry Applications*, vol. 36, no. 4, pp. 1069–1076, 2000.

[5] R. S. Raheem, M. Y. Hassan, and S. K. Kdahim, "Particle swarm optimization based interval type 2 fuzzy logic control for motor rotor position control of artificial heart pump," *Indonesian Journal of Electrical Engineering and Computer Science*, vol. 25, no. 2, pp. 814–824, 2022.

[6] A. A. Yousif, A. M. Mohammed, and M. M. E. Ali, "Radial force cancellation of bearingless brushless direct current motor using integrated winding configuration," *Indonesian Journal of Electrical Engineering and Computer Science*, vol. 25, no. 1, pp. 79–88, 2022, doi: 10.11591/ijeecs.v25.i1.pp79-88.

[7] A. Yousif, A. Mohammed, and M. M. Ali, "Eccentricity effect on radial forces of bearingless BLDC motor: study and analysis," *Engineering and Technology Journal*, vol. 40, no. 2, pp. 358–368, 2022, doi: 10.30684/etj.v40i2.2218.

[8]   R. Raheem, M. Y., and S. Kadhim, "Simulation design of blood-pump intelligent controller based on PID-like fuzzy logic technique," *Engineering and Technology Journal*, vol. 38, no. 8, pp. 1200–1213, 2020, doi: 10.30684/etj.v38i8a.534.

[9]   X. Sun, H. Zhu, and T. Zhang, "Dynamic decoupling control for radial position of bearingless induction motor based on neural networks inverse system," *2009 IEEE 6th International Power Electronics and Motion Control Conference, IPEMC '09*, pp. 602–606, 2009, doi: 10.1109/IPEMC.2009.5157457.

[10]   Y. K. Jelbaoui, E. M. Lamiaà, and A. Saad, "Fault diagnosis of a squirrel cage induction motor fed by an inverter using Lissajous curve of an auxiliary winding voltage," *Indonesian J. Electr. Eng. Comput. Sci*, vol. 21, p. 1299, 2021.

[11]   W. Bu, X. Zhang, and F. He, "Sliding mode variable structure control strategy of bearingless induction motor based on inverse system decoupling," *IEEJ Transactions on Electrical and Electronic Engineering*, vol. 13, no. 7, pp. 1052–1059, 2018, doi: 10.1002/tee.22663.

[12]   K. Li, G. Cheng, X. Sun, D. Zhao, and Z. Yang, "Direct torque and suspension force control for bearingless induction motors based on active disturbance rejection control SCHeme," *IEEE Access*, vol. 7, pp. 86989–87001, 2019, doi: 10.1109/ACCESS.2019.2925359.

[13]   J. Lu, Z. Yang, X. Sun, C. Bao, and X. Chen, "Direct levitation force control for a bearingless induction motor based on model prediction," *IEEE Access*, vol. 7, pp. 65368–65378, 2019, doi: 10.1109/ACCESS.2019.2917331.

[14]   Z. Yang, D. Zhang, X. Sun, W. Sun, and L. Chen, "Nonsingular fast terminal sliding mode control for a bearingless induction motor," *IEEE Access*, vol. 5, pp. 16656–16664, 2017, doi: 10.1109/ACCESS.2017.2739199.

[15]   Z. Yang, Q. Ding, X. Sun, H. Zhu, and C. Lu, "Fractional-order sliding mode control for a bearingless induction motor based on improved load torque observer," *Journal of the Franklin Institute*, vol. 358, no. 7, pp. 3701–3725, 2021, doi: 10.1016/j.jfranklin.2021.03.006.

[16]   Z. Yang, K. Wang, X. Sun, and X. Ye, "Load disturbance rejection control of a bearingless induction motor based on fractional-order integral sliding mode," *Proceedings of the Institution of Mechanical Engineers. Part I: Journal of Systems and Control Engineering*, vol. 232, no. 10, pp. 1356–1364, 2018, doi: 10.1177/0959651818782277.

[17]   I. Ferdiansyah, M. R. Rusli, B. Praharsena, H. Toar, Ridwan, and E. Purwanto, "Speed control of three phase induction motor using indirect field oriented control based on real-time control system," *Proceedings of 2018 10th International Conference on Information Technology and Electrical Engineering: Smart Technology for Better Society, ICITEE 2018*, pp. 438–442, 2018, doi: 10.1109/ICITEED.2018.8534864.

[18]   A. Chiba, T. Fukao, O. Ichikawa, M. Oshima, M. Takemoto, and D. G. Dorrell, "Magnetic bearings and bearingless drives," *Magnetic Bearings and Bearingless Drives*, 2005, doi: 10.1016/B978-0-7506-5727-3.X5000-7.

[19]   Y. Zhou, H. Zhu, and T. Li, "Decoupling control of magnetically levitated induction motor with inverse system theory," in *2006 CES/IEEE 5th International Power Electronics and Motion Control Conference*, 2006, vol. 3, pp. 1–5.

[20]   S. Nomura, A. Chiba, F. Nakamura, K. Ikeda, T. Fukao, and M. A. Rahman, "A radial position control of induction type bearingless motor considering phase delay caused by the rotor squirrel cage," *Proceedings of Power Conversion Conference - Yokohama 1993*, pp. 438–443, 1993, doi: 10.1109/PCCON.1993.264144.

[21]   Z. Yang, X. Sun, M. Wang, and H. Zhu, "Decoupling control of bearingless induction motors based on least squares support vector machine inverse," *Journal of Computational and Theoretical Nanoscience*, vol. 11, no. 5, pp. 1403–1409, 2014, doi: 10.1166/jctn.2014.3510.

[22]   W. Bu, X. Tu, C. Lu, and Y. Pu, "Adaptive feedforward vibration compensation control strategy of bearingless induction motor," *International Journal of Applied Electromagnetics and Mechanics*, vol. 63, no. 2, pp. 199–215, 2020, doi: 10.3233/JAE-190092.

[23]   E. A. D. F. Nunes *et al.*, "Proposal of a fuzzy controller for radial position in a bearingless induction motor," *IEEE Access*, vol. 7, pp. 114808–114816, 2019.

[24]   M. A. Hannan, J. A. Ali, A. Mohamed, U. A. U. Amiru111din, N. M. L. Tan, and M. N. Uddin, "Quantum-behaved lightning search algorithm to improve indirect field-oriented fuzzy-PI control for im drive," *IEEE Transactions on Industry Applications*, vol. 54, no. 4, pp. 3793–3805, 2018, doi: 10.1109/TIA.2018.2821644.

[25]   N. Farah *et al.*, "Fuzzy membership functions tuning for speed controller of induction motor drive: Performance improvement," *Indonesian Journal of Electrical Engineering and Computer Science*, vol. 23, no. 3, pp. 1258–1270, 2021, doi: 10.11591/ijeecs.v23.i3.pp1258-1270.

[26]   H. Zhu, Z. Yang, X. Sun, D. Wang, and X. Chen, "Rotor vibration control of a bearingless induction motor based on unbalanced force feed-forward compensation and current compensation," *IEEE Access*, vol. 8, pp. 12988–12998, 2020, doi: 10.1109/ACCESS.2020.2964106.

BIOGRAPHIES OF AUTHORS

Qasim Kadhim Jasim was born in Babylon, Iraq in 1978. He received a Bachelor's degree in Electrical Engineering from Babylon University, Iraq in 2005. He is currently studying toward a Master's degree of Science in Electrical Power Engineering at the University of Technology, Iraq. He can be contacted at email: eee.20.70@grad.uotechnology.edu.iq.

Mohammed Moanes E. Ali was born in Baghdad, Iraq in 1971. He received the B.Sc., M.Sc., and Ph.D. degrees in electrical engineering from University of Technology, Iraq in 1994, 1997, and 2009, respectively. Since May 2006, he has been with the Department of Electrical Engineering-University of Technology, where he was an Assist. Lect., became a Lecturer in 2009, and an Assist. Prof. in 2018.His current research interests include Electro heat (induction heating), Electrical Machines, and Drives. Mohammed Moanes published more than thirty technical papers. He can be contacted at email: mohammedmoanes.e.ali@uotechnology.edu.iq.